

Article

# Effect of Remelting Temperature and Soaking Time on Microstructure and Mechanical Properties of the Thixoformed Part of Nano-Sized SiCp/7075 Composite

Jufu Jiang <sup>1,\*</sup>, Guanfei Xiao <sup>1</sup>, Yingze Liu <sup>1</sup>, Ying Wang <sup>2,\*</sup> and Xi Nie <sup>1</sup>

<sup>1</sup> School of Materials Science and Engineering, Harbin Institute of Technology, Harbin 150001, China; guanfeixiao@163.com (G.X.); liuyingze1995@foxmail.com (Y.L.); niexihg@163.com (X.N.)

<sup>2</sup> School of Mechatronics Engineering, Harbin Institute of Technology, Harbin 150001, China

\* Correspondence: jiangjufu@hit.edu.cn (J.J.); wangying1002@hit.edu.cn (Y.W.); Tel.: +86-18746013176 (J.J.); +86-15945697615 (Y.W.)

Received: 5 August 2018; Accepted: 7 September 2018; Published: 11 September 2018



**Abstract:** Semisolid billet of the 7075 aluminum matrix composite reinforced with nano-sized SiC particles was first fabricated by an ultrasonic-assisted semisolid stirring method and rheoforming technology. Then it was thixoformed into a cylinder part under different remelting temperatures and soak times. The effects of the remelting temperature and soaking time on the mechanical properties and microstructure of the thixoformed composite part were investigated. The results show that parts of good quality were thixoformed successfully. The microstructure of the top side wall of the thixoformed part consisted of near spheroidal grains. A large quantity of elongated grains occurred in the medium and bottom side walls and the bottom itself. With increasing remelting temperatures, the size of the solid grains of the thixoformed parts showed a trend of first to increase and afterwards to decrease. High density dislocations were found in the microstructure when the remelting temperatures were 590 °C and 600 °C. When the soaking time was 15 min, the severest deformation occurred in the thixoformed part. High mechanical properties of the thixoformed parts were achieved under conditions such as a remelting temperature between 590 °C and 600 °C and a soaking time between 10 min and 15 min. The fracture mode of the thixoformed part changed from transgranular fracture to intergranular fracture when the remelting temperature was elevated from 580 °C to 610 °C. After the thixoformed parts were treated by T6, the ultimate tensile strength (UTS) and elongation of the side wall were improved to 552 MPa and 7.9%, respectively. Dispersed MgZn<sub>2</sub> precipitates created by T6 heat treatment led to an improvement of the mechanical properties.

**Keywords:** nano-sized SiC particles; 7075 aluminum alloy; microstructure; mechanical properties; thixoforming

## 1. Introduction

Semisolid processing (SSP) developed by M.C. Flemings and D.B. Spencer from the MIT is a typical near-net-shape technology [1,2]. It has exhibited an obvious advantage versus conventional casting and forging [3]. Two typical forming technologies are involved in SSP, rheoforming and thixoforming. The rheoforming is referred to as a forming technology in which a semisolid slurry with spheroidal solid grains and liquid phase is carried directed into the die cavity and formed into the final part. The thixoforming is defined as a forming technology in which a semisolid slurry with spheroidal solid grains and liquid is first fabricated, solidified into solid billet, quantitatively cut, reheated to semisolid temperature, and formed into the final parts. In the thixoforming, fabricated semisolid

billet with spheroidal grains surrounded by liquid phase undergoes a remelting process and forming process. The fabricated methods of semisolid billet include mechanical stirring [4,5], electromagnetic stirring [6,7], strain induced melt activated (SIMA) [8–10], as well as recrystallization and partial remelting (RAP) [11,12]. Thixoforming exhibits low resistance to deformation and a good ability to fill die cavity because of the spheroidal grains surrounded by liquid phase. The materials used in the thixoforming process involve aluminum alloys, magnesium alloys, high melting point alloys, and composites. Especially for difficult-deform magnesium alloy, thixoforming was found to be a promising route to obtain parts with high performance [13,14].

Casting and wrought aluminum alloys are perfectly applicable for thixoforming of high-performance products. A large amount of research was focused on thixoforming of a variety of cast and wrought aluminum alloys. Research on 7075 aluminum alloy compound forming technology proposed via combining thixoforming and plastic deformation showed that the harness was almost uniform in spite of the different microstructures in the formed parts [15]. Examining the influence of the processing route on the microstructure of thixoformed A356 alloy, Kaio et al. [16] found that samples prepared by the equal channel angular pressing (ECAP) route were suitable for thixoforming. The effect of different process parameters on thixoextrusion of A357 aluminum alloy was investigated [17]. It was concluded that A357 alloy with high solid fraction more than 0.85 allowed more stable material flow at higher speeds. The mechanical properties of the thixoformed A380 aluminum alloy were improved significantly compared to cast alloy [18]. A390 aluminum alloy with 40–50% fraction liquid were near-net shaped into complex automotive components by using thixoforming [19]. The highest yield strength and elongation were obtained in the thixoformed 7075 wrought alloys in a simple graphite die [20]. In addition, 6061 [21], 2014 [22] and 6082 [23] wrought aluminum alloys were also used for thixoforming and showed good thixoformability.

Magnesium alloys, as another typical light alloy, were used as materials for thixoforming. The mechanical properties of thixoformed AM60B alloys fabricated by the cyclic extrusion compression (CEC) method were higher than those of thixoformed AM60B alloys prepared by the compression and partial remelting method [24]. Higher mechanical properties were obtained in the thixoformed product of AZ80 magnesium alloy fabricated by the new SIMA method compared to conventional SIMA and semisolid isothermal treatment [25]. High melting point alloys are also used as thixoforming materials. Omar et al. [26] revealed that the HP9/4/30 steel product were thixoformed successfully in the range of 1470–1480 °C. Forming load was also highly repeatable as long as the flow was kept laminar, as reported by Pierret et al. [27]. Composites are also suitable for thixoforming. Cheng et al. [28] reported the effect of solution treatment on the microstructure and properties of thixoformed  $Mg_2Si_p/AM60B$  composite. They found that the tensile properties increased with increasing solution time from 0 h to 6 h. Semisolid processing shows an obvious advantage in preparing and forming composites reinforced with ceramic particles [29–31]. The reinforcements in these composites are mainly micro-sized ceramic particles.

In recent years, nano-sized ceramic particles such as SiC and  $Al_2O_3$  have been used to reinforce a metal matrix, so-called nano-sized ceramic particle reinforced aluminum matrix composites (NCPRAMCs) [32–34]. An electromagnetic stirring method was employed to fabricate NCPRAMCs reinforced with a variety of nano-sized ceramic particles such as TiC,  $Al_2O_3$ , and  $B_4C$  [35–40]. In addition, adaptive-network-based fuzzy inference system (ANFIS) and particle swarm optimization (PSO) were used to optimize the process parameters such as mold temperature, mix time, size of reinforcement, and volume fraction of reinforcement [35–40]. How to disperse uniformly the nano-sized ceramic particles is a challenging problem for the fabrication of NCPRAMCs. A new method called ultrasonic-assisted semisolid stirring (UASS) was proposed to solve the dispersion of nano-sized SiC particles during the fabrication of the composite semisolid slurry. In order to fabricate high-quality semisolid slurry of 7075 aluminum matrix composite reinforced with nano-sized SiC particles, the optimal parameters including stirring temperature of 620 °C and stirring time of 20 min were obtained, as reported by Jiang et al. [41]. Furthermore, the effect of stirring time

and pressure on mechanical properties and microstructure were reported in previous research of Jiang et al. [42]. Besides rheofforming, thixoforming is also a promising technology for forming NCPAMCs [43]. Thixoforming has exhibited some obvious advantages such as lower resistance to deformation of materials and easier formation of structure components of a complex shape as compared to conventional forging technology. In addition, it also gives an advantage of achieving higher mechanical properties compared to conventional casting technology. However, research on thixoforming of aluminum matrix composite reinforced with nano-sized ceramic particles has been seldom reported. Therefore, the present research aimed to investigate thixoforming of 7075 aluminum matrix composite reinforced with nano-sized SiC particles in order to determine the effect of remelting temperature and soaking time on the microstructure and mechanical properties of the thixoformed parts produced from the nano-sized SiCp/7075 nanocomposite.

## 2. Materials and Methods

Wrought 7075 aluminum alloys supplied by Northeast Light Alloy Co. Ltd. of China (Harbin, China) were used as matrix material of the composite. Its chemical composition was analyzed with an Axios pw4400 X-ray fluorescence spectrometer (PANalytical B.V., Almelo, The Netherlands) and contained 6.0 wt% Zn, 2.3 wt% Mg, 1.56 wt% Cu, 0.26 Si wt%, 0.27 wt% Mn, 0.17 wt% Cr, 0.03 wt% Ti and balance of Al. Nano-sized SiC particles with an average size of 80 nm were used as reinforcement of the composite. It was supplied by Xuzhou Jiechuang New Materials Co. Ltd. of China (Xuzhou, China). The solidus of 546 °C and liquidus of 637 °C temperatures were determined by using a Differential Thermal Analyzer (Mettler-Toledo, Zurich, Switzerland) [41]. Solid fractions at various temperatures were obtained by integrating the data of the differential scanning calorimetry (DSC) converted from DTA data [36]. The 7075 aluminum alloy was first melted at 650 °C via a molybdenum crucible placed in a resistance furnace. In order to compensate for the loss of Mg element due to evaporation or formation of Mg oxides, a small pure Mg ingot accounting for 0.2 wt% of the total weight of 7075 alloy was added into the melt. The melt was held isothermally for 10 min. Then nano-sized SiC particles were added into the melt of 7075 alloy. The melt with nano-sized SiC particles was treated for 20 min via a 2 kw ultrasonic device at a frequency of 20 kHz. After that, the 7075 alloy with nano-sized SiC particles was stirred continuously with a molybdenum stirrer when it was cooled from 650 °C (above the liquidus temperature) to 620 °C (a given semisolid temperature). When the 7075 alloy with nano-sized SiC particles was cooled to 620 °C, it was stirred isothermally for 20 min to fabricate a semisolid slurry of composite. The semisolid billet of nano-sized SiCp/7075 composite was fabricated by rheofforming the semisolid slurry via a 2000 kN hydraulic press and a die with a preheated temperature of 300 °C [41]. Figure 1 shows the macrograph of the fabricated semisolid billet of the nano-sized SiCp/7075 composite. Thixoforming experiments were carried out on a designed die with a preheating temperature of 400 °C. The die schematic diagram and real product for the thixoforming cylinder part were given in the previous research of Jiang et al. [42]. The applied load and pressure-holding time during the thixoforming process were 2000 kN and 10 s, respectively. Three groups of thixoforming experiments were performed. In the first group, semisolid billets soaked for 5 min, 10 min, 15 min, 20 min, and 25 min respectively were thixoformed at 580 °C. In the second group, semisolid billets soaked for 5 min, 10 min, 15 min, 20 min, and 25 min respectively were thixoformed at 600 °C. In the third group, semisolid billets soaked for 10 min were thixoformed at 580 °C, 590 °C, 600 °C, and 610 °C, respectively.

The microstructural specimens were cut from the locations as shown in Figure 2a, then ground with 200, 400, 600, 800, 1200, and 2000 grit papers, and polished with 0.1 µm diamond paste. The specimens were etched for about 10 s by Keller's reagent (4 mL HF, 6 mL HCL, 8 mL HNO<sub>3</sub> and 82 mL water) and observed by using an Olympus GX71 optical microscope (Olympus Coporation, Tokyo, Japan), Quanta 200 FEI scanning electron microscope (FEI, Hillsboro, OR, USA) equipped with an energy dispersive X-ray spectrometer (EDX) and Jeol2100 (Tokyo, Japan) transmission electron microscope (TEM) and a Talos F200x (FEI, Hillsboro, OR, USA) TEM with Energy Dispersive X-ray

spectrometers (EDS). Tensile specimens were cut from the locations as shown in Figure 2b and then machined into standard tensile specimens according to ASTM Standard Test Methods for Tension Testing of Metallic Materials, E8M [44]. Some tensile specimens were directly tested at room temperature. The other specimens were first heat treated in solution for 6 h at 465 °C with ageing for 18 h at 125 °C and then used for the tensile test.



**Figure 1.** Macrograph of the fabricated semisolid billet of the nano-sized SiCp/7075 composite via rheoforming of the semisolid slurry prepared by ultrasonic-assisted semisolid stirring (UASS).

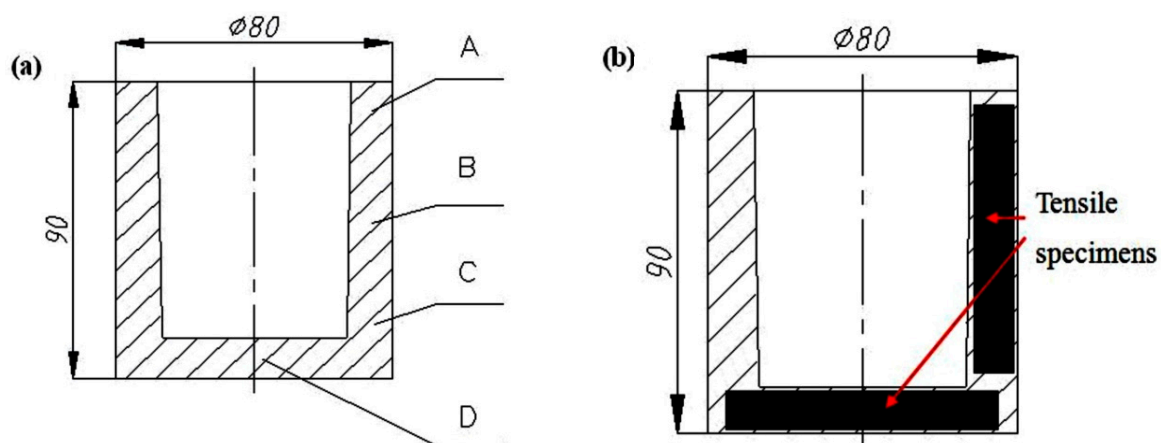


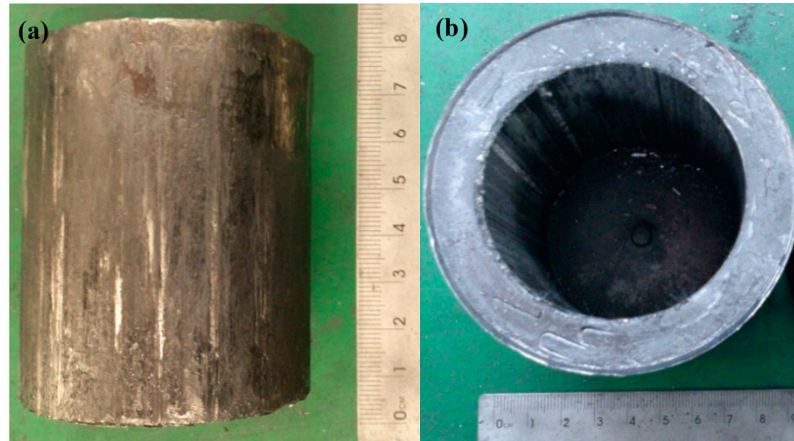
**Figure 2.** Sampling schematic diagram of the (a) microstructural specimens and (b) the tensile specimens.

### 3. Results and Discussion

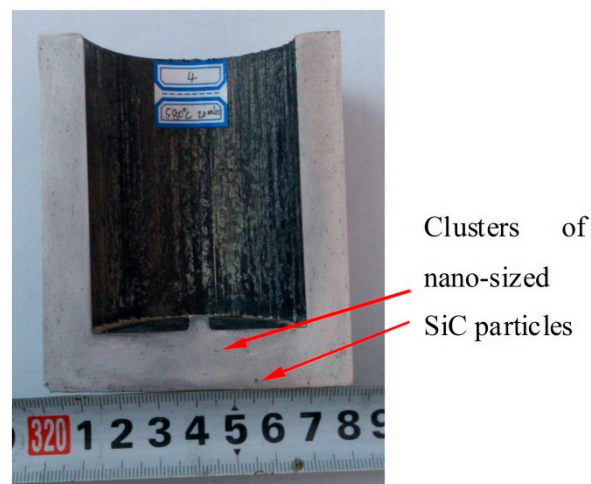
Figure 3 shows the macrograph of the thixoformed part of the nano-sized SiCp/7075 composite. As indicated in Figure 3, a cylinder part was thixoformed successfully due to good filling ability of the semisolid billet. Good surface quality was observed in the thixoformed part. A half-sectional macrograph is shown in Figure 4. As shown in Figure 4, the macrostructure of the thixoformed part is very dense and no obvious porosity was found in the macrostructure. In addition, it is noticeable that slight clusters of nano-sized SiC particles are found in the macrostructure. It illustrates that absolutely perfect dispersion of the nano-sized SiC particles in the 7075 alloy matrix is very difficult to obtain although transient cavitation and acoustic streaming created by an ultrasonic wave and high and controllable viscosity of the semisolid slurry can disperse the nano-sized SiC particles effectively. Therefore, some slight clusters were found in the matrix due to large Van der Waals forces and electrostatic forces between the nano-sized SiC particles (Figure 4).

Figure 5 gives the optical metalloscope (OM) and scanning electron microscope (SEM) microstructure in different locations of the thixoformed part of the nano-sized SiCp/7075 composite soaked for 10 min at 590 °C. As shown in Figure 5a,d, the microstructure consists of solid grains

and liquid phase. Fine, near spheroidal solid grains and elongated solid grains along the flowing direction of the semisolid slurry were found in the microstructure of the thixoformed part. The fine microstructure of the semisolid slurry fabricated by the ultrasonic-assisted semisolid stirring method led to the fine solid grains of the thixoformed part [41].



**Figure 3.** Macrographs of the thixoformed part of the nano-sized SiCp/7075 composite: (a) front view and (b) top view.



**Figure 4.** Half-sectional macrograph of the thixoformed part of the nano-sized SiCp/7075 composite.

The microstructure consisting of fine grains is beneficial for improving the mechanical properties of the thixoformed part. In addition, it can be seen that the solid grains in location A almost keep a near spheroidal shape (Figure 5a). However, the solid grains in the locations B, C, and D were obviously elongated along the flowing direction of semisolid slurry (Figure 5b–d). The high resolution SEM exhibited a homogeneous dispersion of nano-sized SiC particles (Figure 5e). There are four deformation mechanisms in the semisolid compression process, liquid flow (LF), flow of liquid incorporating solid grains (FLS), sliding between solid grains (SSS), and plastic deformation of solid grains (PDS) [45]. The top side wall (location A) of the cylinder part has a free surface without limits of die during the medium stage of thixoforming [42]. Its deformation mode belongs to liquid flow (LF), flow of liquid incorporating solid grains (FLS), and sliding between solid grains (SSS). Therefore, the solid grains almost remain spheroidal shape after deformation. However, the deformation modes in locations B, C, and D belong to plastic deformation of solid grains (PDS). As a consequence, this resulted in the elongated grains after deformation.

In addition, it can be seen that the liquid fraction in the microstructure decreases with a location change from A to D. The liquid fraction in location A is obviously higher than those in locations B, C, and D. A similar phenomenon was found in the microstructure of the rheoformed cylinder parts of nano-sized SiCp/7075 composite [42]. The difference between them is that the extent of change of the liquid fraction in the thixoformed part is less than that in the rheoformed part. This is attributed to the lower remelting temperature in the thixoforming process compared to the rheoforming process shown in the previous research [42]. The amount of liquid phase influences the deformation mechanism in a difference location. In location A, liquid phase is aggregated obviously due to lower flowing resistance as compared with solid grains, resulting in the occurrence of FLS or SSS deformation mechanisms. Compared with location A, the amount of liquid phase in locations B, C, and D decreases obviously due to its segregation in location A. Consequently, the deformation mechanism of PDS is dominant during the flow of semisolid slurry.

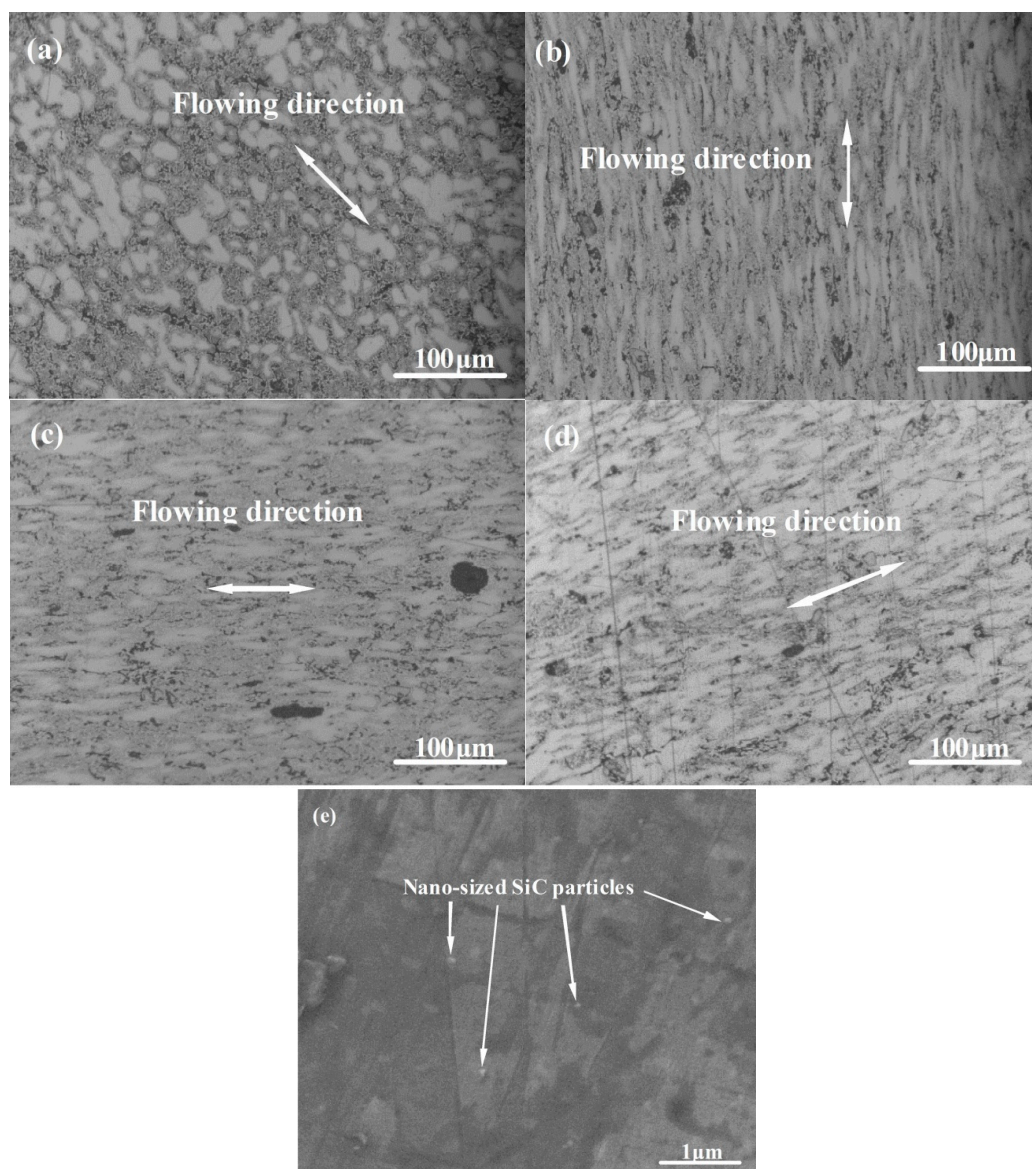


**Figure 5.** Microstructure in different locations of the thixoformed part of the nano-sized SiCp/7075 composite soaked for 10 min at 590 °C: (a) Optical microscopy (OM) image in location A; (b) OM image in location B; (c) OM image in location C; (d) OM image in location D and (e) scanning electron microscopy (SEM) image in location C.

Figure 6 shows the OM microstructure in location B of the thixoformed parts of the nano-sized SiCp/7075 composite soaked for 10 min at different remelting temperatures. As indicated in Figure 6, the solid grains are elongated obviously along the flowing direction. The grain size of the thixoformed part slightly changes when the remelting temperature increases from 580 °C to 590 °C. However, the grain size of the thixoformed part increases obviously when the remelting temperature is elevated to 600 °C. This is due to the fact that elevated remelting temperature leads to coarsening of the microstructure of the semisolid billet during the remelting process. Therefore, the coarsened solid grains remain in the microstructure of the thixoformed parts. Grain size decreases upon remelting at a temperature of 610 °C. The coarsening trend and melting trend together influence the grain size of the semisolid billet during the remelting process [46]. When the remelting temperature is 610 °C, the melting trend is dominant. Therefore, this leads to a decrease of grain size of the semisolid billet during the remelting process. After the semisolid billet was thixoformed, the grain size of the thixoformed parts slightly decreased. On the whole, the size of the solid grains in the semisolid slurry exhibits first an increase, followed by a decrease with increasing remelting temperatures. This was attributed to the double effect of coarsening trend and melting trend caused by increasing the remelting temperatures. In addition, it is also noticeable that nano particles are slightly clustered in Figures 5 and 6. This was attributed to large Van der Waals force and electrostatic force between nano-sized SiC particles. Therefore, absolutely homogeneous dispersion of nano-sized is not possible to obtain due to the large Van der Waals and electrostatic forces between the nano-sized SiC particles.

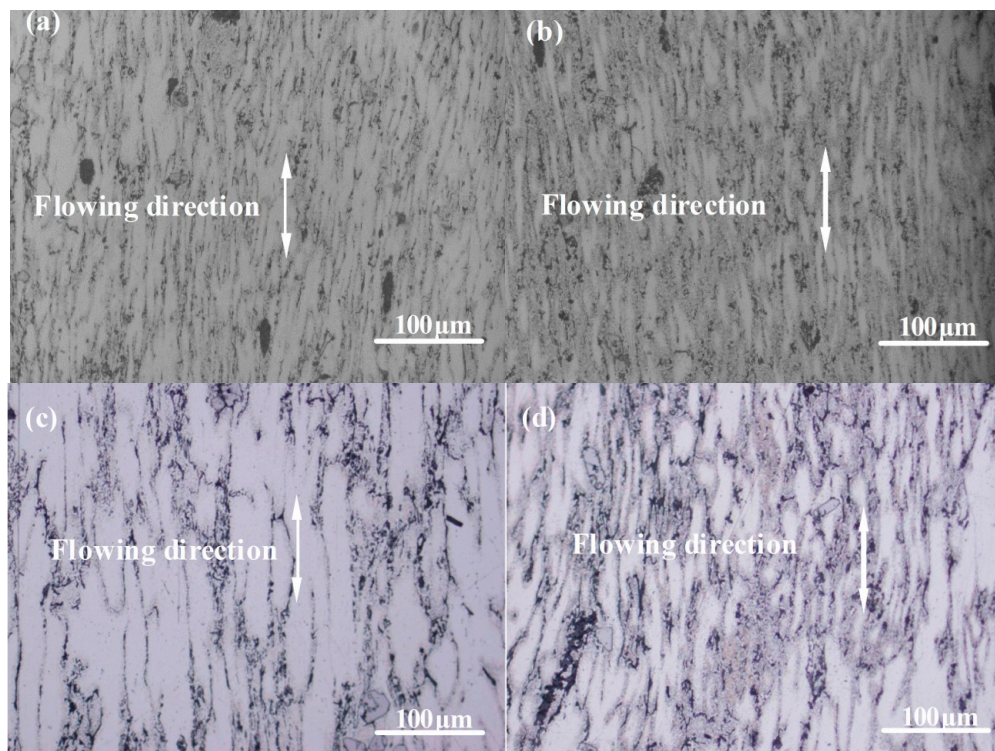


**Figure 6.** OM microstructure in location B of the thixoformed parts of the nano-sized SiCp/7075 composite soaked for 10 min at different remelting temperatures: (a) 580 °C, (b) 590 °C, (c) 600 °C, and (d) 610 °C.

Figure 7 shows the mechanical properties of the thixoformed parts of the nano-sized SiCp/7075 composite soaked for 10 min at different remelting temperatures. As indicated in Figure 7, the ultimate tensile strength (UTS) of the side wall of the thixoformed part only slightly increases when the remelting temperature increases from 580 °C to 590 °C. However, the UTS decreases gradually upon further increase of the remelting temperature. The highest UTS of 313 MPa was obtained at a remelting temperature of 590 °C. The highest elongation of 5.4% of the thixoformed part was achieved at a

remelting temperature of 600 °C. It can be noted that the UTS and elongation of the side wall of the thixoformed part are higher than those at the bottom of the thixoformed part. As to the mechanical properties at the bottom of the thixoformed parts, the highest UTS and elongation of the thixoformed parts were achieved at a remelting temperature of 600 °C. According to the UTS and elongation of the thixoformed parts, the optimal remelting temperatures should be 590 °C and 600 °C.

The liquid fraction influences the deformation degree of solid grains during the thixoforming process. It can be noted that the liquid fraction increases with an increase of remelting temperature. When the remelting temperatures are 580 °C, 590 °C, 600 °C, and 610 °C, the liquid fractions are 0.19, 0.3, 0.38 and 0.49 respectively [41]. Therefore, the liquid fractions at remelting temperatures of 580 °C and 590 °C are less than those at 600 °C and 610 °C. The contact extent between solid grains becomes large due to a small amount of liquid phase at a low remelting temperature. As a consequence, larger deformation occurs in the solid grains, leading to more obvious strain strengthening.

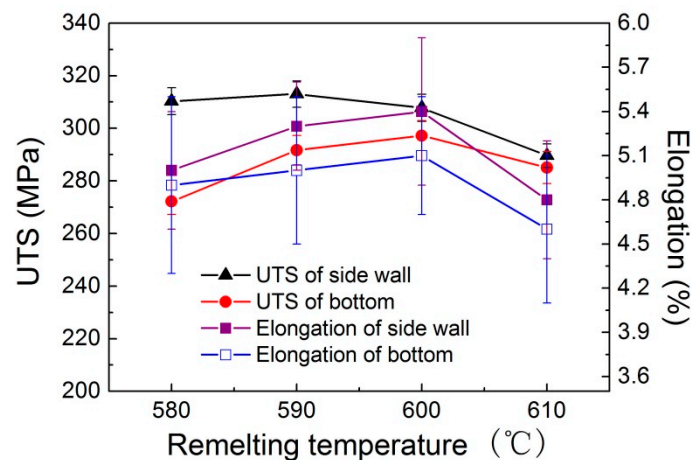


**Figure 7.** Mechanical properties of the thixoformed parts of the nano-sized SiCp/7075 composite soaked for 10 min at different remelting temperatures.

Figure 8 gives evidence of the dislocations created in the thixoformed composite parts at different remelting temperatures. More dislocations were created due to large deformation, which can improve the UTS by hindering grain sliding. As shown in Figure 8, a large amount of high density dislocations were found in the microstructure of the thixoformed composite parts at 580 °C, 590 °C, and 600 °C. An obvious dislocation wall was created in the microstructure of the thixoformed composite part at 610 °C. This was attributed to dynamic recovery occurring in the deformation process, leading to a decreased dislocation density. It is also consistent with the decreased UTS of the thixoformed composite at 610 °C (Figure 7). Especially, high density dislocations were noted in the thixoformed composite at 590 °C. This illustrates that the highest UTS of the side wall was obtained at 590 °C. Furthermore, as shown in Figure 6, the deformation degree of the thixoformed part at 590 °C is larger than those at 580 °C, 600 °C, and 610 °C. In addition, fine grains also improve the UTS of the thixoformed part according to the Hall–Petch effect [47].

The microstructure of the thixoformed part soaked for different times at 600 °C is presented in Figure 9. As indicated in Figure 9, a large number of elongated grains were found in the microstructure. Furthermore, the elongated extent of the solid grains with a soaking time of 15 min is the largest, illustrating the largest deformation degree. This led to improvement of UTS and elongation of the thixoformed part (see Figure 10). Therefore, the highest mechanical properties of the thixoformed part are achieved with a soaking time of 15 min. When the soaking time is 20 min and 25 min, obvious liquid phase segregation was found in the microstructure, which led to a reduction of mechanical properties. Unlike the mechanical properties of the thixoformed part with elevated remelting temperature, no obvious regulation was found in the mechanical properties of the thixoformed part soaked for different times at 600 °C.

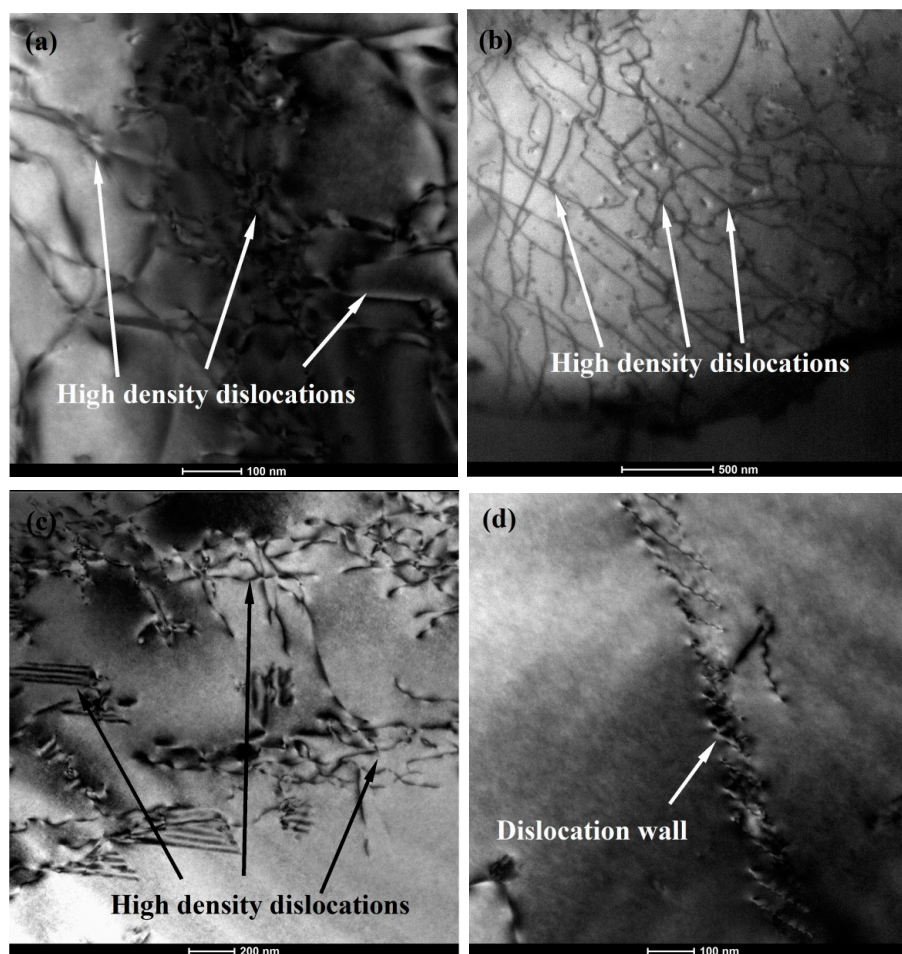


**Figure 8.** Transmission electron microscopy (TEM) images in location B of the thixoformed composite parts at different remelting temperatures (a) 580 °C, (b) 590 °C, (c) 600 °C, (d) 610 °C.

Figure 11 and Table 1 give an EDX analysis result of the thixoformed part soaked for 10 min at 590 °C. This illustrates the existence of nano-sized SiC in the nano-sized SiCp/7075 composite. Furthermore, it can be noticed that nano-sized SiC particles in the grain boundaries are more than those in the grains. Mg and Zn elements in the grain boundaries are less than those in the interior of the grains. This indicates the  $\eta$  phase ( $\text{MgZn}_2$ ) mainly exists in the grain boundaries, leading to some consumption of Mg and Zn elements in the grain boundaries. It is noticeable that Cu element aggregated in the grain boundaries.

The solid phase consisted of the  $\alpha$ -Al phase containing more of Al element and less of other alloying elements such as Zn, Mg, and Cu. The chemical composition of the solid phase is given in Table 1. The liquid phase consisted of the  $\alpha$ -Al phase containing less Al element and more other alloying elements such as Zn, Mg, and Cu and the second phase such as  $\eta$  phase ( $\text{MgZn}_2$ ) and T phase ( $\text{Al}_2\text{Mg}_3\text{Zn}_3$ ). The chemical composition of the liquid phase is shown in Table 1.

High-resolution TEM micrograph and EDX results are presented in Figure 12. Tables 2 and 3 exhibit the elements in locations A and B. As indicated in Table 1, the phase contains C and Si elements, implying the existence of nano-sized SiC particles. However, the matrix phase ( $\alpha$ -Al) does not contain Si element. As shown in Figure 12, nano-sized SiC particles are distributed uniformly in the microstructure. It also illustrates that the ultrasonic-assisted semisolid stirring method is suitable for fabricating a semisolid slurry of the nano-sized SiCp/7075 composite.

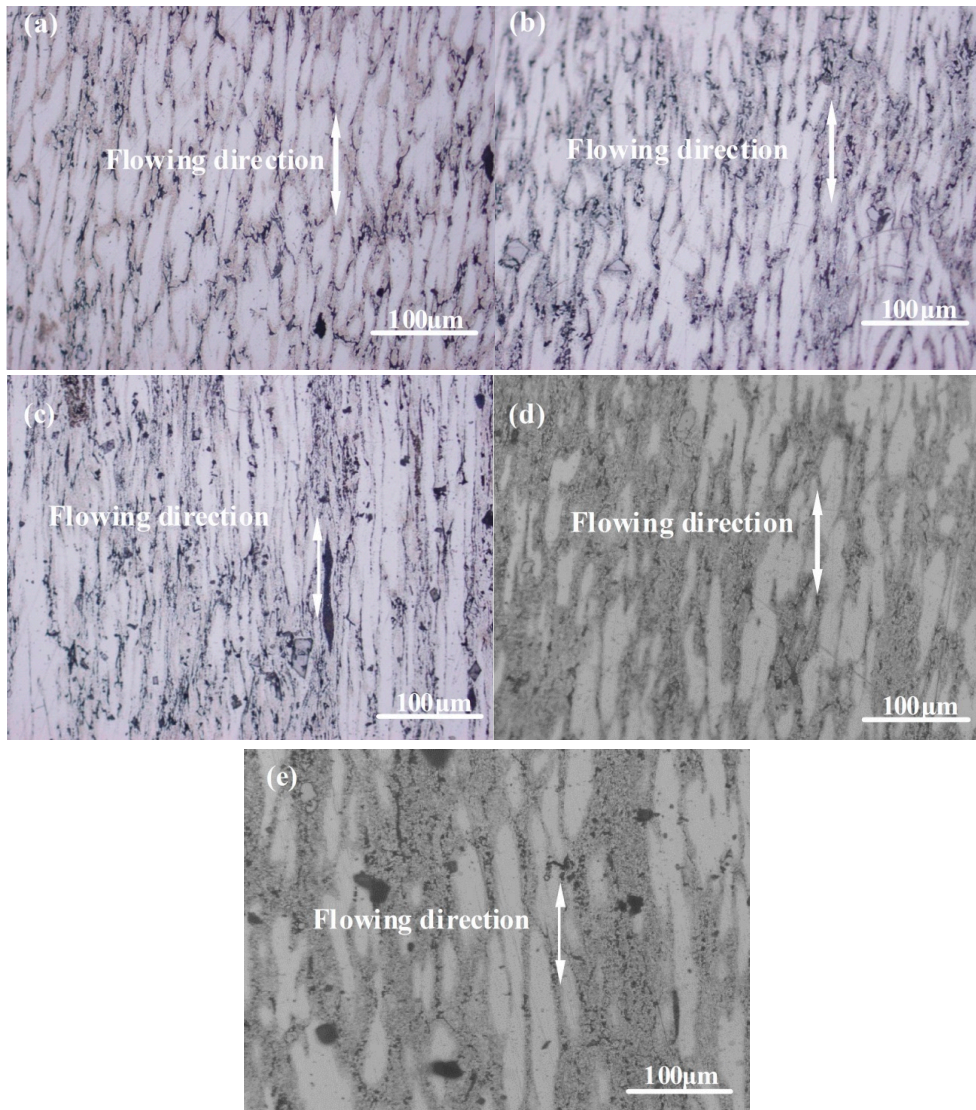


**Figure 9.** OM microstructure of the thixoformed part soaked for different times at 600 °C: (a) 5 min, (b) 10 min, (c) 15 min, (d) 20 min, and (e) 25 min.

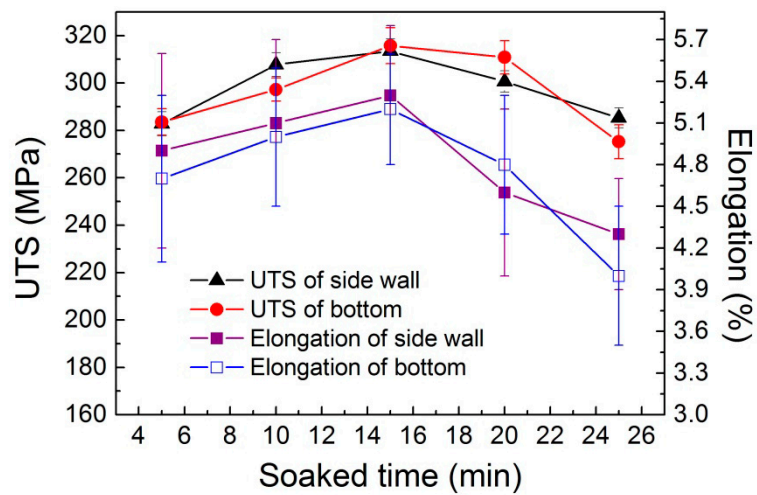


**Figure 10.** Mechanical properties of the thixoformed part soaked for different times at 600 °C.

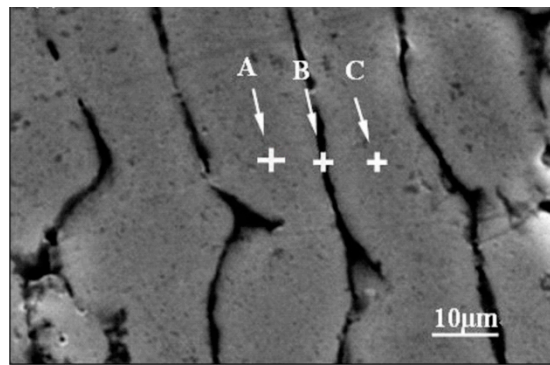


**Figure 11.** Positions of energy dispersive X-ray spectrometry (EDX) analysis of the thixoformed part soaked for 10 min at 590 °C.

**Table 1.** Energy dispersive X-ray spectrometry (EDX) results in different locations of the thixoformed part soaked for 10 min at 590 °C.

Elements		Al	Zn	Mg	Cu	Si	C
Position A	wt%	88.91	5.51	3.08	0.88	0.58	1.04
	at%	90.86	2.32	3.49	0.38	0.57	2.38
Position B	wt%	86.13	4.77	2.56	1.12	2.81	2.62
	at%	86.13	1.97	2.84	0.47	2.70	5.88
Position C	wt%	89.52	5.07	2.77	0.98	0.25	1.40
	at%	91.07	2.07	3.04	0.41	0.24	3.18

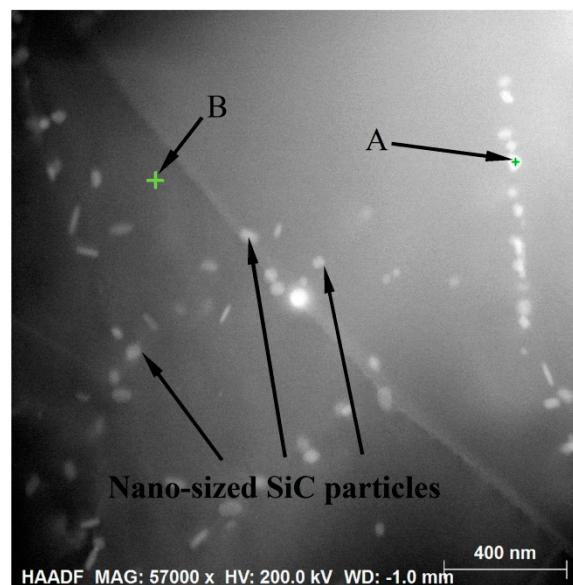


**Figure 12.** High-resolution TEM micrograph of the thixoformed part soaked for 10 min at 590 °C.

**Table 2.** Element in location A of the thixoformed part soaked for 10 min at 590 °C.

Element	Series	Net	(wt%)	(norm. wt%)	(norm. at%)	Error in wt%
Carbon	K-series	3216	2.49	2.49	5.69	0.332
Aluminum	K-series	269,060	87.22	87.22	88.84	7.942
Copper	K-series	5101	2.74	2.74	1.18	0.352
Chromium	K-series	1031	0.47	0.47	0.25	0.14
Manganese	K-series	4941	2.08	2.08	1.04	0.29
Iron	K-series	8962	3.90	3.90	1.92	0.45
Silicon	K-series	3469	1.10	1.10	1.08	0.13
		Sum	100	100	100	

**Table 3.** Element in location B of the thixoformed part soaked for 10 min at 590 °C.

Element	Series	Net	(wt%)	(norm. wt%)	(norm. at%)	Error in wt%
Carbon	K-series	69,567	12.21	12.21	23.96	1.18
Aluminum	K-series	1,174,789	86.43	86.43	75.52	7.86
Chromium	K-series	596	0.06	0.06	0.03	0.08
Manganese	K-series	749	0.08	0.08	0.04	0.09
Copper	K-series	10,023	1.22	1.22	0.45	0.19
		Sum	100	100	100	

Figure 13 gives the tensile fracture at the bottom of the thixoformed parts soaked for 10 min at different remelting temperatures. As indicated in Figure 13a, some obvious small-sized dimples and quasi-cleavage steps are simultaneously found in the fracture of the thixoformed part. This illustrates a mixed fracture of the ductile fracture and the brittle fracture occurring in the tensile specimens.

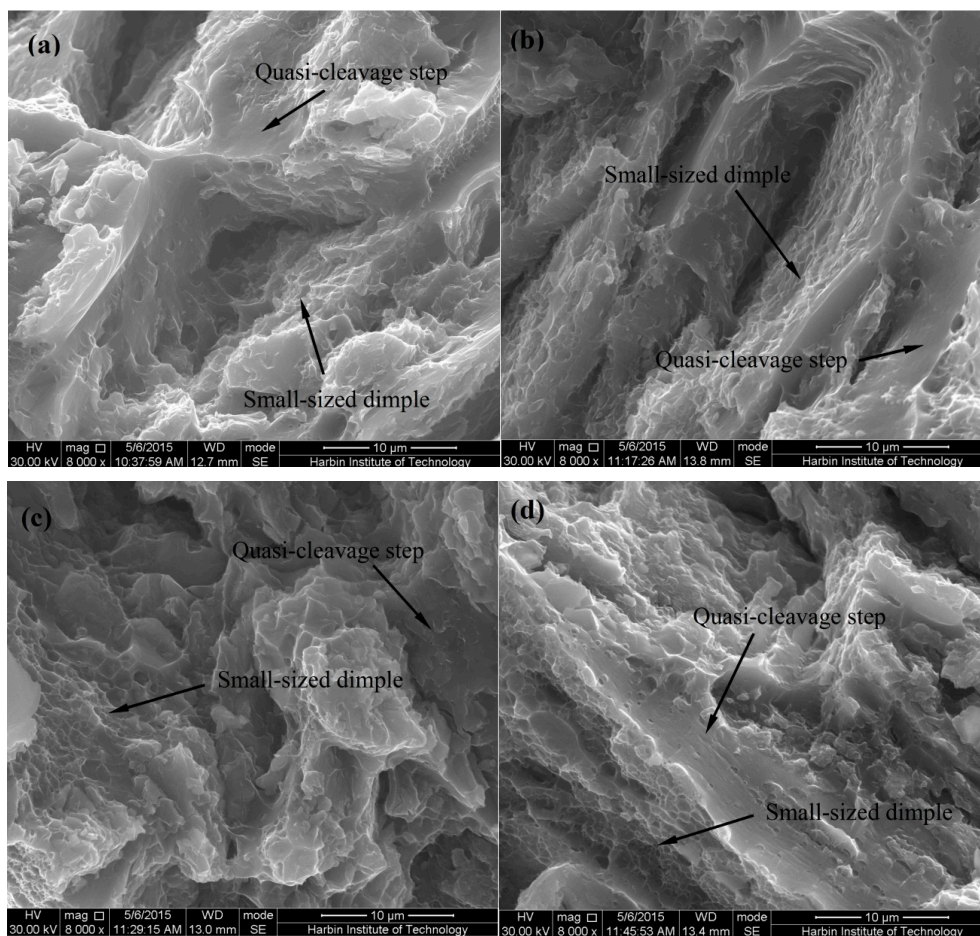


**Figure 13.** Tensile fracture at the bottom of the thixoformed parts soaked for 10 min at different remelting temperatures: (a) 580 °C, (b) 590 °C, (c) 600 °C, and (d) 610 °C.

Figure 14 shows the OM images of the fracture of the bottom of thixoformed part soaked for 10 min at different remelting temperatures. The fracture type of the thixoformed part at 580 °C is transgranular fracture (Figure 14a). Intergranular fracture and transgranular fracture occurred together in the thixoformed part at 590 °C (Figure 14b). When the remelting temperature is elevated to 600 °C and 610 °C, obvious intergranular fracture was found in the fracture macrograph (Figure 14c,d). This is due to the effect of increasing liquid film thickness and liquid segregation. When the remelting temperature is elevated, increased liquid fraction leads to an increase of liquid film thickness and

liquid segregation. The strength in the areas of the liquid film and liquid segregation is lower than the solid grain's strength, resulting in easier occurrence of fracture compared with solid grains.

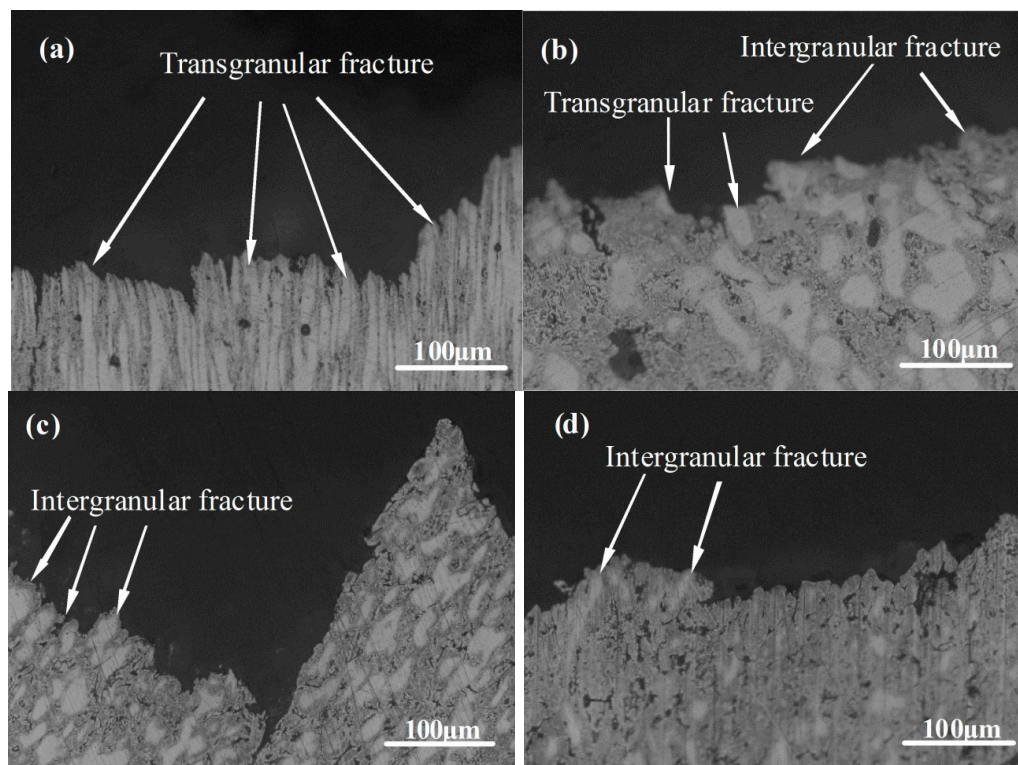


**Figure 14.** Macrograph of the fracture at the bottom of the thixoformed part soaked for 10 min at different remelting temperatures: (a) 580 °C, (b) 590 °C, (c) 600 °C, and (d) 610 °C.

Figure 15 gives the effect of T6 treatment (i.e., solid solution and artificial aging) on the mechanical properties of the rheoformed composite parts, the thixoformed composite parts, and the thixoformed 7075 aluminum alloy parts. As shown in Figure 15, the mechanical properties were improved significantly after the thixoformed composite parts were treated by T6. The UTS and elongation of the side wall of the thixoformed part without T6 were 313 MPa and 5.4%, respectively. After the thixoformed parts were treated by T6, the UTS and elongation of the side wall were improved to 552 MPa and 7.9%, respectively. The UTS of the thixoformed composite part with T6 was 76.4% higher than that of the thixoformed composite part without T6. The elongation of the thixoformed composite part with T6 was 46.3% higher than that of the thixoformed composite part without T6. The UTS of the bottom of the thixoformed part was increased from 310 MPa to 549 MPa. The elongation increased from 5.3% to 7.8%. The extents of increase were 77% and 47.2%, respectively. The UTS of the thixoformed parts with and without T6 was improved compared to the thixoformed parts of 7075 aluminum alloy with and without T6 due to the addition of nano-sized SiC particles. The increasing dislocation density created by the coefficient of thermal expansion (CTE) mismatch between the matrix and nano-sized particles enhances the strength of the composite [48]. The obstacle of uniformly distributed SiC particles to the movement of dislocation also plays an important role in the improvement of strength according to the Orowan mechanism [49]. In addition, the improvement of strength of the thixoformed parts could be related to the fracture toughness of the interface between the nano-sized SiC and the Al matrix. The pillar splitting technique as reported by Matteo Ghidelli et al. could provide a feasible method to measure the fracture toughness [50]. The elongation of the thixoformed parts with and without T6 was reduced compared with the thixoformed parts of 7075 aluminum alloy with and without T6. The UTS of the thixoformed parts without T6 is less than that of the rheoformed parts without T6 [42]. However, the UTS of the thixoformed composite parts with T6 is even more than that

of the rheoformed composite part with T6. The elongations of the thixoformed composite parts with and without T6 were less than those of the rheoformed composite part with and without T6.

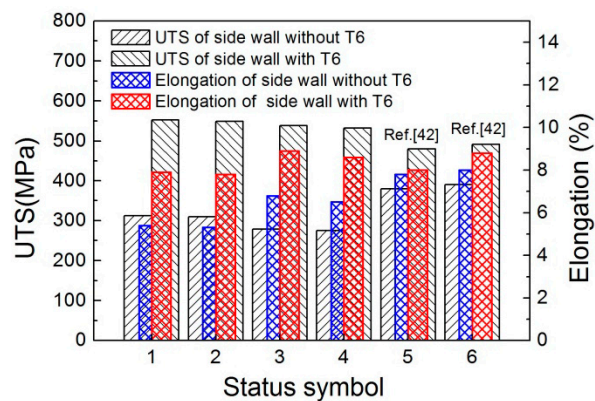


**Figure 15.** Effect of T6 on the mechanical properties of the rheoformed composite parts, the thixoformed composite parts, and thixoformed 7075 aluminum alloy parts. 1 means side wall of the thixoformed composite part, 2 means bottom of the thixoformed composite part, 3 means side wall of the thixoformed 7075 aluminum alloy, 4 means bottom of the thixoformed 7075 aluminum alloy, 5 means side wall of the rheoformed composite part and 6 means the bottom of the rheoformed composite part.

In addition, T6 treatment can make phase ( $MgZn_2$ ) precipitate uniformly in the matrix, as shown in Figure 16. Some long striped  $\eta$  phases ( $MgZn_2$ ) were also found in the TEM micrograph (Figure 16). These  $\eta$  phases ( $MgZn_2$ ) were dissolved in the 7075 alloy matrix after the thixoformed composite parts were solution treated for 6 h at 465 °C. They formed a supersaturated solid solution of  $\alpha$  Al when the solution treated thixoformed parts were quenched. These  $\eta$  phases ( $MgZn_2$ ) precipitated uniformly in the 7075 alloy matrix. The uniformly dispersed  $\eta$  phases strengthen the alloy, leading to improvement of the mechanical properties.

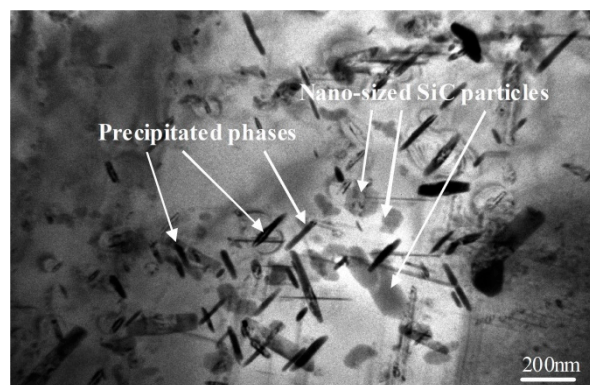


**Figure 16.** TEM micrograph of the thixoformed part soaked for 10 min at 590 °C with T6.

#### 4. Conclusions

- Nano-sized SiCp/7075 composite cylinder parts with good surface quality and dense microstructure were obtained via thixoforming technology. The deformation mechanism of the top side wall depends mainly on the liquid flow (LF), the flow of liquid incorporating solid grains (FLS), and sliding between solid grains (SSS). The plastic deformation (PDS) mechanism dominates the deformation of the middle side wall, the bottom side wall, and the bottom itself.
- The optimal process parameters obtained according to the UTS and elongation results are soaking time between 10 min and 15 min and remelting temperatures between 590 °C and 600 °C. The highest UTS and elongation of the thixoformed composite part without T6 were 313 MPa and 5.4% respectively.

- A mixed fracture morphology was found in the SEM image of tensile fracture due to the simultaneous existence of some small-sized dimples and quasi-cleavage steps. The fracture of the composite part thixoformed at 580 °C is characterized by transgranular fracture. A mixed fracture of transgranular fracture and intergranular fracture was found in the composite part thixoformed at 590 °C. The intergranular fracture was dominant in the composite parts thixoformed at 600 °C and 610 °C due to increasing liquid film thickness and liquid segregation.
- The mechanical properties were improved significantly after the thixoformed composite parts were treated by T6. The highest UTS of 552 MPa and the highest elongation of 7.9% were obtained in the thixoformed composite parts treated by T6. Uniform precipitation of  $\eta$  phase (MgZn<sub>2</sub>) after T6 led to improvement of the mechanical properties of the thixoformed composite part. The UTS of the thixoformed parts with and without T6 was improved compared with the thixoformed 7075 alloy parts with and without T6 due to the addition of nano-sized SiC particles. The UTS of the thixoformed parts with T6 was higher than that of the rheoformed composite part.

**Author Contributions:** J.J. designed most experiments, analyzed the results, and wrote this manuscript. G.X., Y.L., and X.N. performed most experiments. Y.W. helped analyze the experimental data and gave some constructive suggestions of how to write the manuscript.

**Acknowledgments:** This research was funded by the Natural Science Foundation of China (NSFC) by Grant No.51375112 and the fund of the State Key Laboratory of Advanced Processing and Recycling of Non-ferrous Metals, Lanzhou University of Technology under Grant No.SKLAB02015003.

**Conflicts of Interest:** The authors declare no conflicts of interest.

## References

1. Spencer, D.B. Rheology of liquid-solid mixtures of lead-tin. Ph.D. Thesis, Massachusetts Institute of Technology, Massachusetts, MA, USA, 1971.
2. Spencer, D.B.; Mehrabian, R.; Flemings, M.C. Rheological behavior of Sn-15 pct Pb in the crystallization range. *Metall. Trans. B* **1972**, *3*, 1925–1932. [[CrossRef](#)]
3. Flemings, M.C. Behavior of metal alloys in the semisolid state. *Metall. Trans. A* **1991**, *22*, 957–981. [[CrossRef](#)]
4. Haghayeghi, R.; Zoqui, E.J.; Halvae, A.; Emamy, M. An investigation on semi-solid Al-7Si-0.3Mg alloy produced by mechanical stirring. *J. Mater. Process. Technol.* **2005**, *169*, 382–387. [[CrossRef](#)]
5. Li, D.N.; Luo, J.R.; Wu, S.S.; Xiao, Z.H.; Mao, Y.W.; Song, X.J.; Wu, G.Z. Study on the semi-solid rheocasting of magnesium alloy by mechanical stirring. *J. Mater. Process. Technol.* **2002**, *129*, 431–434. [[CrossRef](#)]
6. Wang, C.L.; Chen, A.T.; Zhang, L.; Liu, W.C.; Wu, G.H.; Ding, W.J. Preparation of an Mg-Gd-Zn alloy semisolid slurry by low frequency electro-magnetic stirring. *Mater. Des.* **2015**, *84*, 53–63. [[CrossRef](#)]
7. Bai, Y.L.; Xu, J.; Zhang, Z.F.; Shi, L.K. Annulus electromagnetic stirring for preparing semisolid A357 aluminum alloy slurry. *Trans. Nonferrous Met. Soc. China* **2009**, *19*, 1104–1109. [[CrossRef](#)]
8. Young, K.P.; Kyonka, C.P.; Courtois, J.A. Fine Grained metal composition. U.S. Patent 4415374, 30 March 1982.
9. Saklakoglu, N.; Saklakoglu, I.E.; Tanoglu, M.; Oztas, O.; Cubukcuoglu, O. Mechanical properties and microstructural evaluation of AA5013 aluminum alloy treated in the semi-solid state by SIMA process. *J. Mater. Process. Technol.* **2004**, *148*, 103–107. [[CrossRef](#)]
10. Bolouri, A.; Shahmiri, M.; Kang, C.G. Coarsening of equiaxed microstructure in the semisolid state of aluminum 7075 alloy through SIMA processing. *J. Mater. Sci.* **2012**, *47*, 3544–3553. [[CrossRef](#)]
11. Kirkwood, D.H.; Sellars, C.M.; Elias Boyed, L.G. Thixotropic Materials. European Patent 0305375 B1, 28 October 1992.
12. Bolouri, A.; Kang, C.G. Correlation between solid fraction and tensile properties of semisolid RAP processed aluminum alloys. *J. Alloys Compd.* **2012**, *516*, 192–200. [[CrossRef](#)]
13. Chen, Q.; Yuan, B.G.; Lin, J.; Xia, X.S.; Zhao, Z.D.; Shu, D.Y. Comparisons of microstructure, thixoformability and mechanical properties of high performance wrought magnesium alloys reheated from the as-cast and extruded states. *J. Alloys Compd.* **2014**, *584*, 63–75. [[CrossRef](#)]
14. Chen, Q.; Zhao, Z.D.; Chen, G.; Wang, B. Effect of accumulative plastic deformation on generation of spheroidal structure, thixoformability and mechanical properties of large-size AM60 magnesium alloy. *J. Alloys Compd.* **2015**, *632*, 190–200. [[CrossRef](#)]

15. Chen, Q.; Chen, G.; Ji, X.H.; Han, F.; Zhao, Z.D.; Wan, J.; Xiao, X.Q. Compound forming of 7075 aluminum alloy based on functional integration of plastic deformation and thixoformation. *J. Mater. Process. Technol.* **2017**, *246*, 167–175. [[CrossRef](#)]
16. Kaio, N.C.; Cecília, T.W.P.; Eugênio, J.Z. Influence of the processing route on the microstructure of aluminum alloy A356 for thixoforming. *Mater. Charact.* **2013**, *85*, 26–37.
17. Forn, A.; Vaneetveld, G.; Pierret, J.C.; Menarguess, S.; Baile, M.T.; Camillom, M.; Rassili, A. Thixoextrusion of A357 aluminium alloy. *Trans. Nonferrous Met. Soc. China* **2010**, *20*, s1005–s1009. [[CrossRef](#)]
18. Parshizfard, E.; Shabestari, S.G. An investigation on the microstructural evolution and mechanical properties of A380 aluminum alloy during SIMA process. *J. Alloys Compd.* **2011**, *509*, 9654–9658. [[CrossRef](#)]
19. Kapranos, P.; Kirkwood, D.H.; Atkinson, H.V.; Rheinlander, J.T.; Bentzen, J.J.; Toft, P.T.; Debel, C.P.; Laslaz, G.; Maenner, L.; Blais, S.; et al. Thixoforming of an automotive part in A390 hypereutectic Al–Si alloy. *J. Mater. Process. Technol.* **2003**, *135*, 271–277. [[CrossRef](#)]
20. Chayong, S.; Atkinson, H.V.; Kapranos, P. Thixoforming 7075 aluminium alloys. *Mater. Sci. Eng. A* **2005**, *390*, 3–12. [[CrossRef](#)]
21. Abolhasani, D.; Ezatpour, H.R.; Sajjadi, S.A.; Abolhasani, Q. Microstructure and mechanical properties evolution of 6061 aluminum alloy formed by forward thixoextrusion process. *Mater. Des.* **2013**, *49*, 784–790. [[CrossRef](#)]
22. Birol, Y. Thixoforming of EN AW-2014 alloy at high solid fraction. *J. Mater. Process. Technol.* **2011**, *211*, 749–756. [[CrossRef](#)]
23. Birol, Y. Comparison of thixoformability of AA6082 reheated from the as-cast and extruded states. *J. Alloys Compd.* **2008**, *461*, 132–138. [[CrossRef](#)]
24. Wang, L.P.; Jiang, W.Y.; Chen, T.; Feng, Y.C.; Zhou, H.Y.; Zhao, S.C.; Liang, Z.Q.; Zhu, Y. Spheroidal microstructure formation and thixoforming of AM60B magnesium alloy prepared by SIMA process. *Trans. Nonferrous Met. Soc. China* **2012**, *22*, s435–s444. [[CrossRef](#)]
25. Jiang, J.F.; Wang, Y.; Qu, J.J.; Du, Z.M.; Luo, S.J. Preparation and thixoforging of semisolid billet of AZ80 magnesium alloy. *Trans. Nonferrous Met. Soc. China* **2010**, *20*, 1731–1736. [[CrossRef](#)]
26. Omar, M.Z.; Palmiere, E.J.; Howe, A.A.; Atkinson, H.V.; Kapranos, P. Thixoforming of a high performance HP9/4/30 steel. *Mater. Sci. Eng. A* **2005**, *395*, 53–61. [[CrossRef](#)]
27. Pierret, J.C.; Rassili, A.; Vaneetveld, G.; Lecote-Beckers, J. Stability of steel thixoforming process. *Trans. Nonferrous Met. Soc. China* **2010**, *20*, s937–s942. [[CrossRef](#)]
28. Cheng, F.L.; Chen, T.J.; Qi, Y.S.; Zhang, S.Q.; Yao, P. Effects of solution treatment on microstructure and mechanical properties of thixoformed Mg<sub>2</sub>SiP/AM60B composite. *J. Alloys Compd.* **2015**, *636*, 48–60. [[CrossRef](#)]
29. Guan, L.N.; Geng, L.; Zhang, H.W.; Huang, L.J. Effects of stirring parameters on microstructure and tensile properties of (ABO<sub>w</sub> + SiCp)/6061Al composites fabricated by semi-solid stirring technique. *Trans. Nonferrous Met. Soc. China* **2011**, *21*, s274–s279. [[CrossRef](#)]
30. Alhawari, K.S.; Omar, M.Z.; Ghazali, M.J.; Salleh, M.S.; Mohammed, M.N. Wear properties of A356/Al<sub>2</sub>O<sub>3</sub> metal matrix composites produced by semisolid processing. *Procedia Eng.* **2013**, *68*, 186–192. [[CrossRef](#)]
31. Zhang, H.W.; Geng, L.; Guan, L.N.; Huang, L.J. Effects of SiC particle pretreatment and stirring parameters on the microstructure and mechanical properties of SiCp/Al-6.8Mg composites fabricated by semi-solid stirring technique. *Mater. Sci. Eng. A* **2010**, *528*, 513–518. [[CrossRef](#)]
32. Koli, D.K.; Agnihotri, G.; Purohit, R. A review on properties, behaviour and processing methods for Al-nano Al<sub>2</sub>O<sub>3</sub> composites. *Procedia Mater. Sci.* **2014**, *6*, 567–589. [[CrossRef](#)]
33. Mazahery, A.; Shabani, M.O. Characterization of cast A356 alloy reinforced with nano SiC composites. *Trans. Nonferrous Met. Soc. China* **2012**, *22*, 275–280. [[CrossRef](#)]
34. Kandemir, S. Microstructure and mechanical properties of A357/SiC noncomposites fabricated by ultrasonic cavitation-based dispersion of ball-milled nanoparticles. *J. Compon. Mater.* **2017**, *51*, 395–404. [[CrossRef](#)]
35. Shamsipour, M.; Pahlevani, Z.; Shabani, M.O.; Mazahery, A. Optimization of the EMS process parameters in compocasting of high-wear-resistant Al-nano-TiC composites. *Appl. Phys. A* **2016**, *122*, 457–471. [[CrossRef](#)]
36. Tofigh, A.A.; Rahimpour, M.R.; Shabani, M.O.; Davami, P. Application of the combined neuro-computing, fuzzy logic and swarm intelligence for optimization of compocast nanocomposites. *J. Compon. Mater.* **2015**, *49*, 1653–1663. [[CrossRef](#)]

37. Shamsipour, M.; Pahlevani, Z.; Shabani, M.O.; Mazahery, A. Squeeze casting of electromagnetically stirred aluminum matrix nanocomposites in semi-solid condition using hybrid algorithm optimized parameters. *Kovove Mater.* **2017**, *55*, 33–43. [[CrossRef](#)]
38. Tofigh, A.A.; Shabani, M.O. Efficient optimum solution for high strength Al alloys matrix composites. *Ceram. Int.* **2013**, *39*, 7483–7490. [[CrossRef](#)]
39. Shabani, M.O.; Rahimipour, M.R.; Tofigh, A.A.; Davami, P. Refined microstructure of compo cast nanocomposites: the performance of combined neuro-computing, fuzzy logic and particle swarm techniques, Neural Computing and Applications. *Neural. Comput. Appl.* **2015**, *26*, 899–909. [[CrossRef](#)]
40. Shabani, M.O.; Heydari, F.; Tofigh, A.A.; Rahimipour, M.R.; Razavi, M.; Mazahery, A.; Davami, P. Wear properties of rheo-squeeze cast aluminum matrix reinforced with nano particulates. *Prot. Met. Phys. Chem. Surfaces* **2016**, *52*, 486–491. [[CrossRef](#)]
41. Jiang, J.F.; Wang, Y. Microstructure and mechanical properties of the semisolid slurries and rheoformed component of nano-sized SiC/7075 aluminum matrix composite prepared by ultrasonic-assisted semisolid stirring. *Mater. Sci. Eng. A* **2015**, *639*, 350–358. [[CrossRef](#)]
42. Jiang, J.F.; Wang, Y. Microstructure and mechanical properties of the rheoformed cylindrical part of 7075 aluminum matrix composite reinforced with nano-sized SiC particles. *Mater. Des.* **2015**, *79*, 32–41. [[CrossRef](#)]
43. Kandemir, S.; Atkinson, H.V.; Weston, D.P.; Hainsworth, S.V. Thixoforming of A356/SiC and A356/TiB<sub>2</sub> nanocomposites fabricated by a combination of green compact nanoparticle incorporation and ultrasonic treatment of the melted compact. *Metall. Mater. Trans. A* **2014**, *45A*, 5782–5798. [[CrossRef](#)]
44. ASTM International. *ASTM Standard E8M, Standard Test Methods for Tension Testing of Metallic Materials [Metric]*; ASTM International: West Conshohocken, PA, USA, 2008.
45. Chen, C.P.; Tsao, C.Y.A. Semi-solid deformation of non-dendritic structure-I. Phenomenological behavior. *Acta Mater.* **1997**, *45*, 1955–1968. [[CrossRef](#)]
46. Jiang, J.F.; Luo, S.J. Reheating microstructure of refined AZ91D magnesium alloy in semi-solid state. *Trans. Nonferrous Met. Soc. China* **2004**, *14*, 1074–1081.
47. Kubotak, K.; Mabuchi, M.; Higashi, K. Review processing and mechanical properties of fine-grained Mg alloys. *J. Mater. Sci.* **1999**, *34*, 2255–2262. [[CrossRef](#)]
48. Zhong, X.L.; Wong, W.L.E.; Gupta, M. Enhancing strength and ductility of magnesium by integrating it with aluminum nanoparticles. *Acta Mater.* **2007**, *55*, 6338–6344. [[CrossRef](#)]
49. Karbalaee, M.; Mirzaee, O.; Baharvandi, H.R. Fabrication and study on mechanical properties and fracture behavior of nanometric Al<sub>2</sub>O<sub>3</sub> particle-reinforced A356 composites focusing on the parameters of vortex method. *Mater. Des.* **2013**, *46*, 199–205. [[CrossRef](#)]
50. Ghidelli, M.; Sebastiani, M.; Johanns, K.E.; Pharr, G.M. Effects of indenter angle on micro-scale fracture toughness measurement by pillar splitting. *J. Am. Ceram. Soc.* **2017**, *100*, 5731–5738. [[CrossRef](#)]

